Supporting Information

One Peptide for Them All: Gold Nanoparticles of Different Sizes Are Stabilized by a Common Peptide Amphiphile

Elena A. Egorova,[1] Mark M.J. van Rijt,[2] Nico Sommerdijk,[3] Gert S. Gooris,[4] Joke A. Bouwstra,[4] Aimee L. Boyle,[1] and Alexander Kros[1]**

1. Department of Supramolecular & Biomaterials Chemistry, Leiden Institute of Chemistry, Leiden University, Leiden, 2333 CC, The Netherlands

2. Laboratory of Physical Chemistry and the Centre for Multiscale Electron Microscopy, Department of Chemical Engineering and Chemistry, Eindhoven University of Technology, Eindhoven, 5600 MB, The Netherlands

3. Radboud Institute for Molecular Life Sciences, Radboud UMC, Nijmegen, 6525 GA, The Netherlands

4. Division of BioTherapeutics, Leiden Academic Centre for Drug Research, Leiden University, Leiden, 2333 CC, The Netherlands

Table of Contents

- Table S1. Sequences and structures of reference peptides used in this study:

	Sequence	Chemical structure
5	CALNN	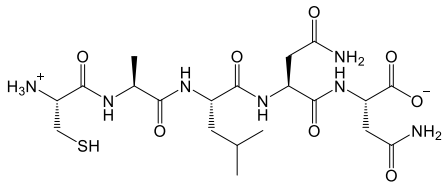
6	CVALNN	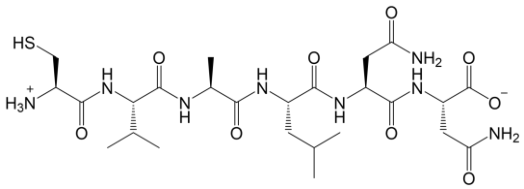
7	CCVVVT	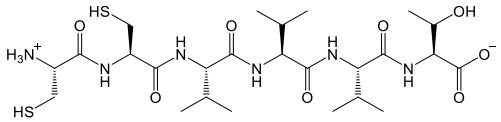
	$C_{16}H_{31}O$-$V_3A_3E_3$	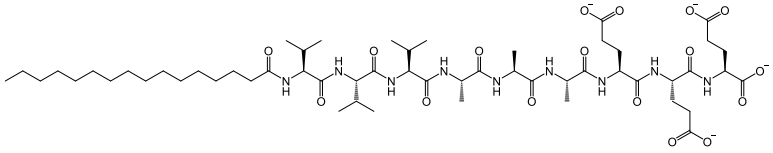

Sequences **5** and **7** were adopted from Levy *et al.*[1] and **6** was designed based on their findings. Sequence $C_{16}H_{31}O$-$V_3A_3E_3$ was taken from Pashuck *et al.*[2]

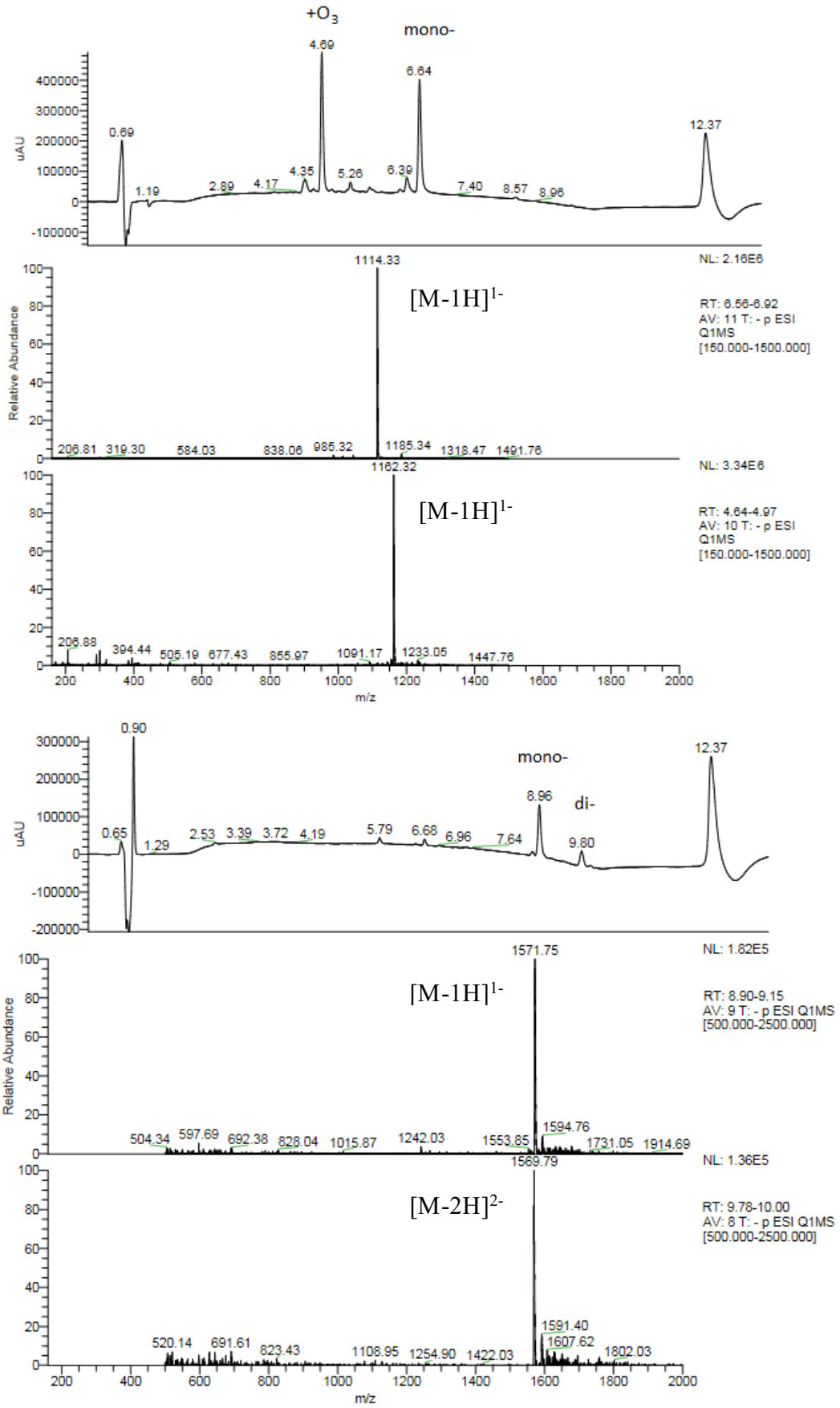

Figure S1. LC-MS data showing dimer formation and oxidation of (A) **2**, and (B) **3** after dissolution in PBS. Dimerization resulted in a decrease in mass of 1 or 2 Da, for single- and double-chain amphiphiles respectively. Oxidation of the terminal thiol was characterized by the appearance of a new peak with a shorter retention time and an increase in mass of 48 Da.

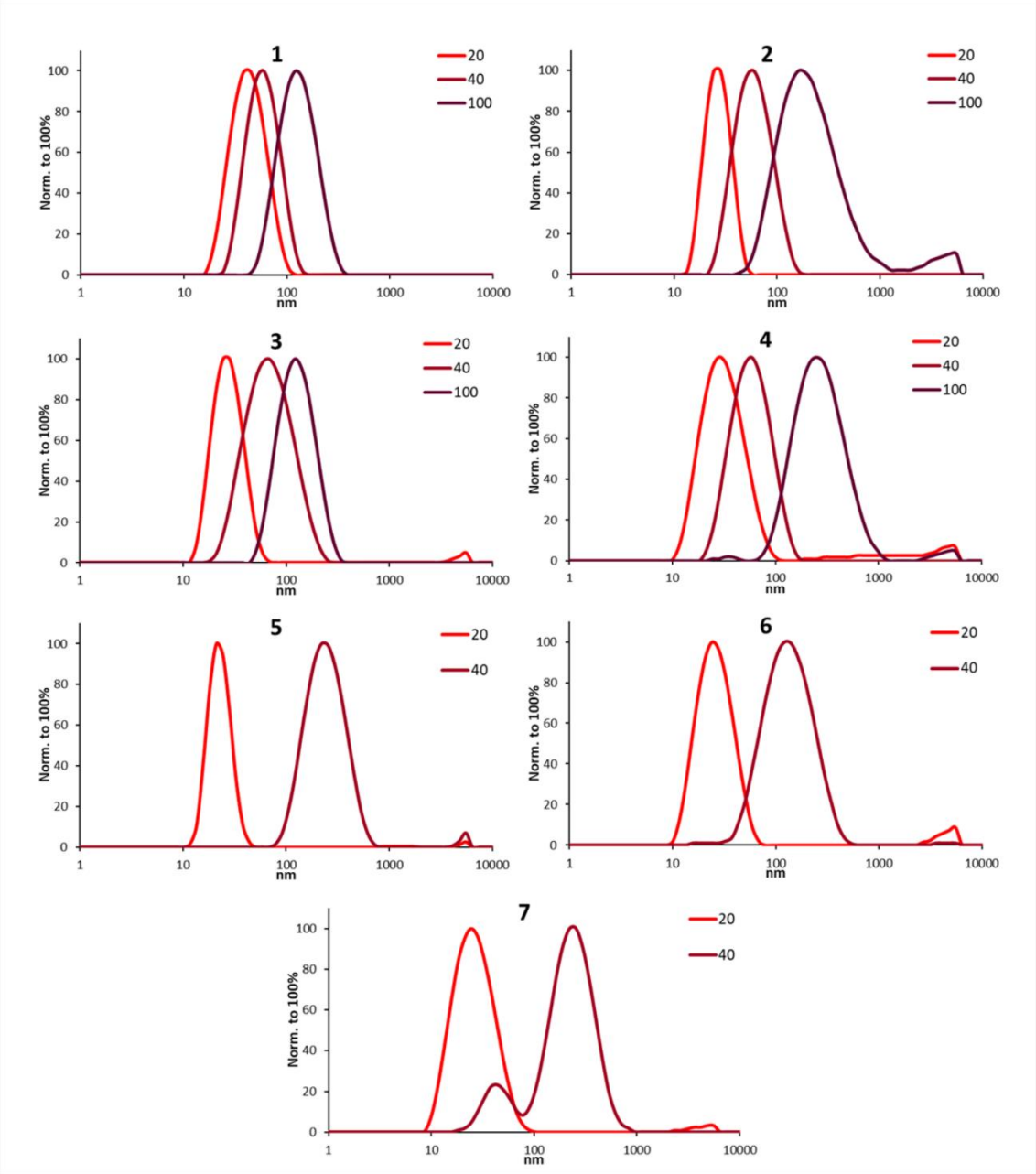

Figure S2. Intensity size distributions by DLS for GNPs functionalized with **1**-**7**. All distributions are normalized to 100%. Measurement conditions: PBS, pH 7.2.

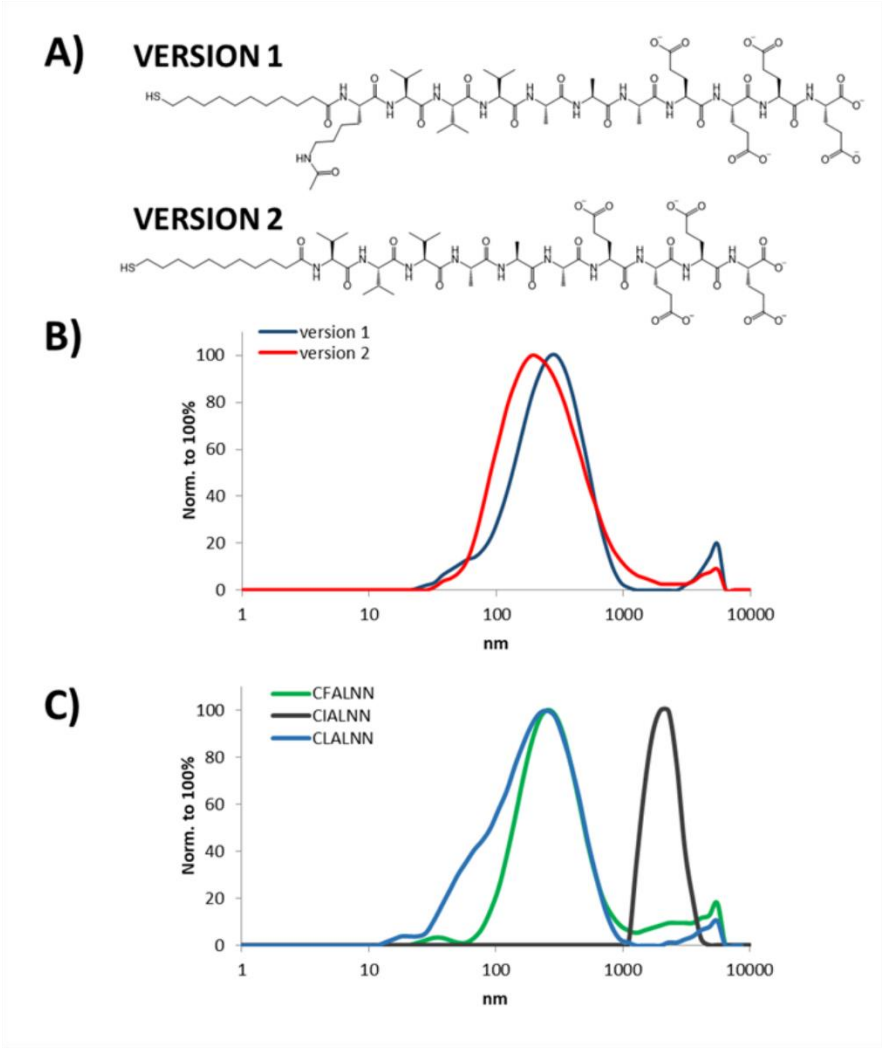

Figure S3. (A) Chemical structures of single-chain analogues of molecule **3**: version 1 contains an acetylated Lys residue (to neutralize the charged side-chain as would occur if an alkyl chain was attached in this position): and version 2, where the Lys residue is omitted. (B) Intensity size distributions by DLS for 100 nm GNPs coated with the two versions of amphiphile **3**. Neither of these molecules stabilize the GNPs, demonstrating the stabilizing effect of **3** is due to the presence of two mercaptoundecanoyl chains. (C) Variants of CVALNN with Phe, Ile, and Leu in place of Val fail to stabilize 40 nm GNPs.
Measurements performed in PBS, pH 7.2. Intensities are normalized to 100%.

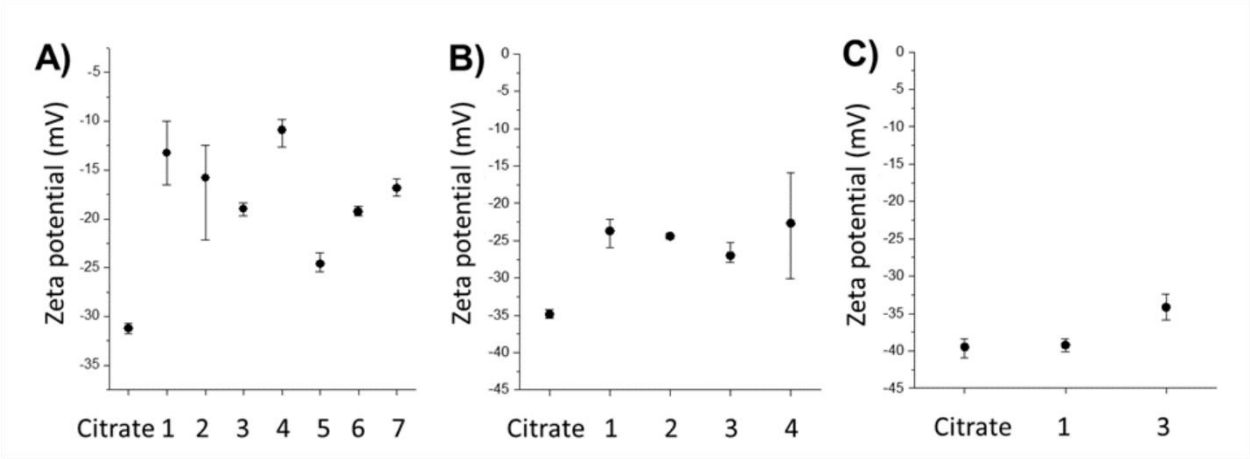

Figure S4. Zeta-potential values for: (A) 20 nm; (B) 40 nm; (C) 100 nm GNPs with citrate and peptide/amphiphile coatings.

Table S2. Average Zeta potential values for citrate- and peptide-/amphiphile-coated GNPs.

Sample	ζ, mV (average)		
	20 nm GNPs	40 nm GNPs	100 nm GNPs
citrate	-31.25	-34,87	-39.47
1	-13.25	-23,70	-39.20
2	-15.83	-24,40	
3	-18.97	-27.00	-34.17
4	-10.93	-22.67	
5	-24.63		
6	-19.27		
7	-16.87		

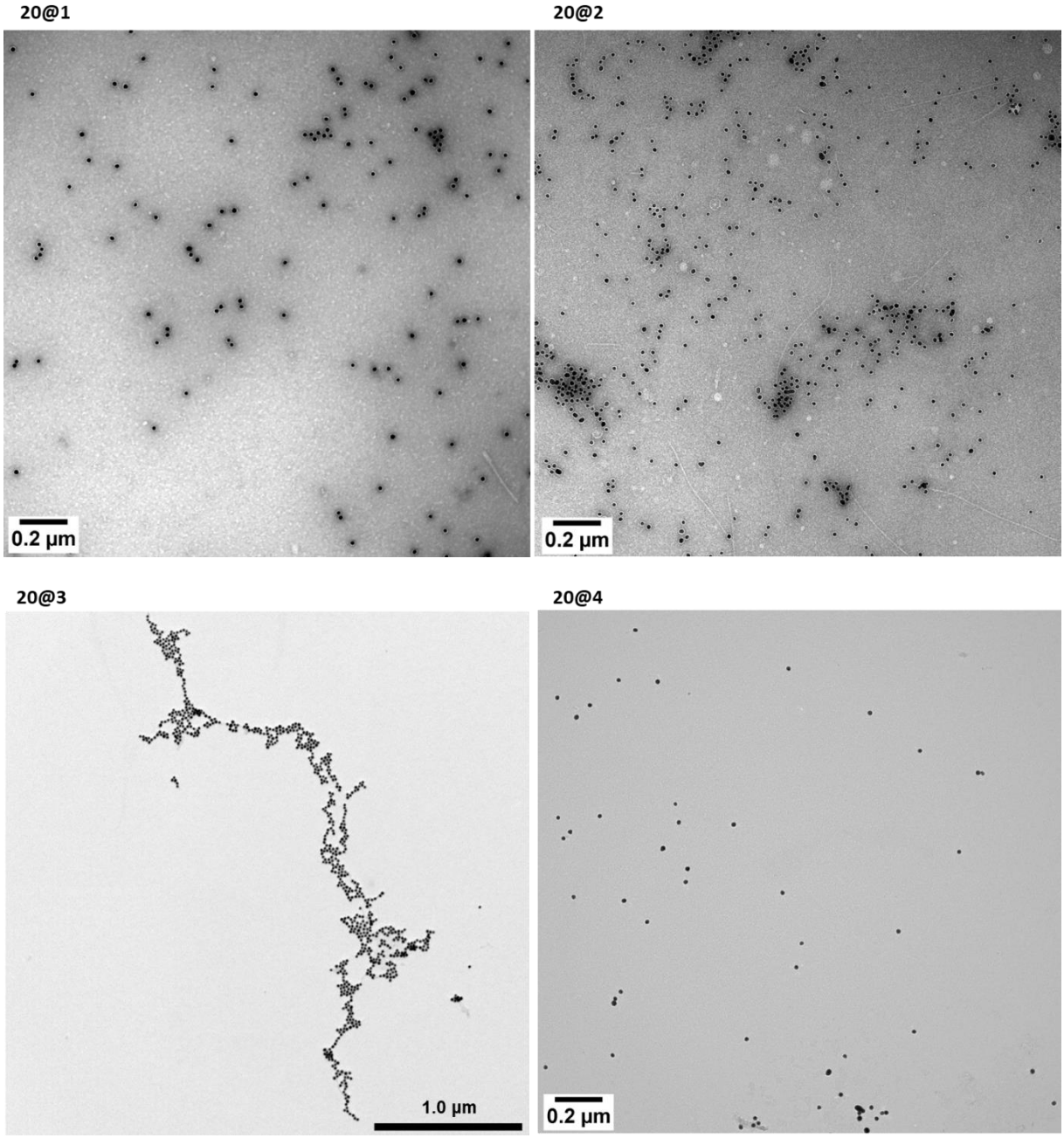

Figure S5. Representative low magnification images of 20 nm GNPs coated with molecules **1**-**4**.

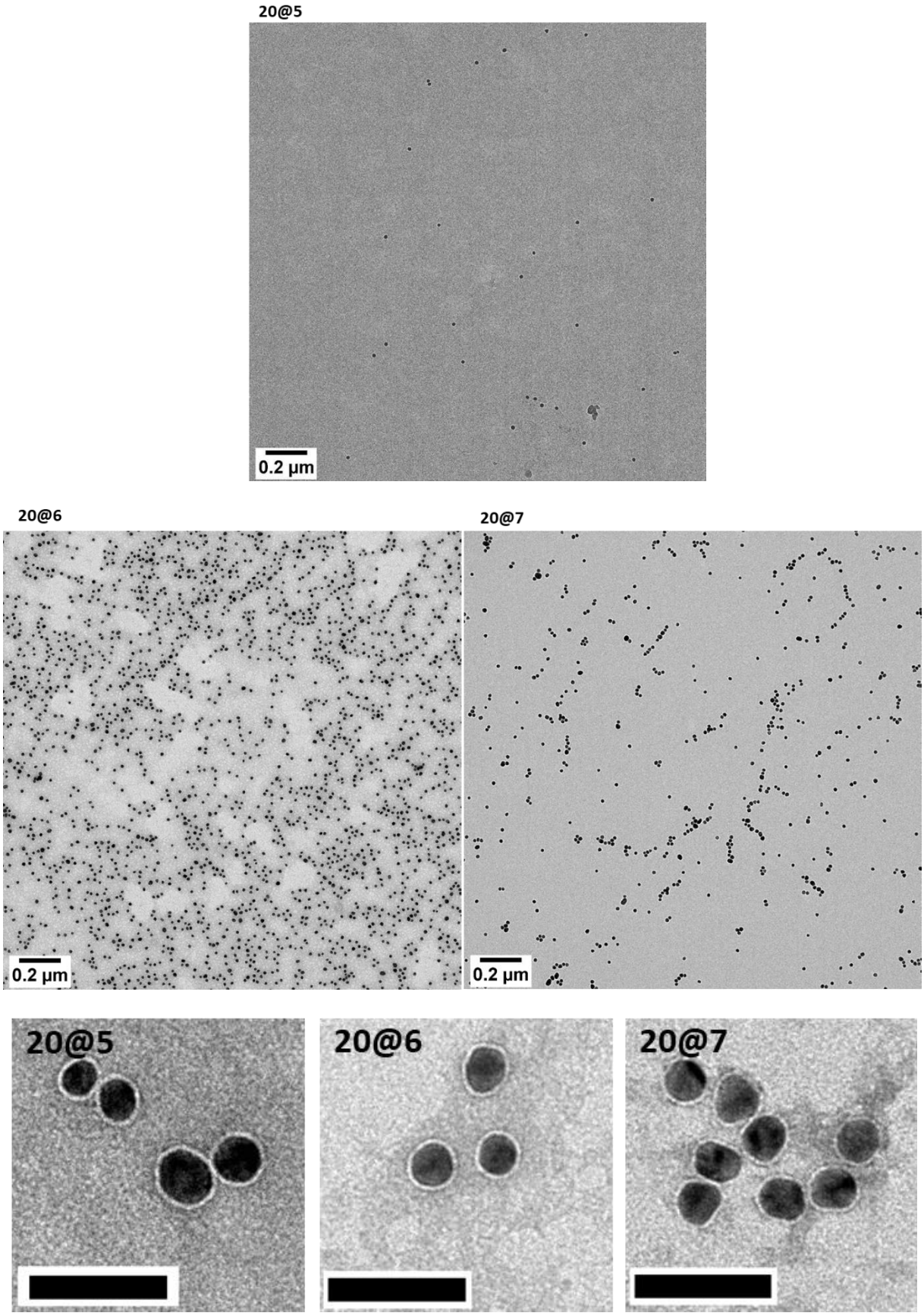

Figure S6. Low magnification images (top & middle) of 20 nm GNPs coated with molecules **5**-**7**. Lower panels: high-magnification images of 20 nm GNPs coated with **5**-**7**. For these lower panels, the scale bar is 50 nm.

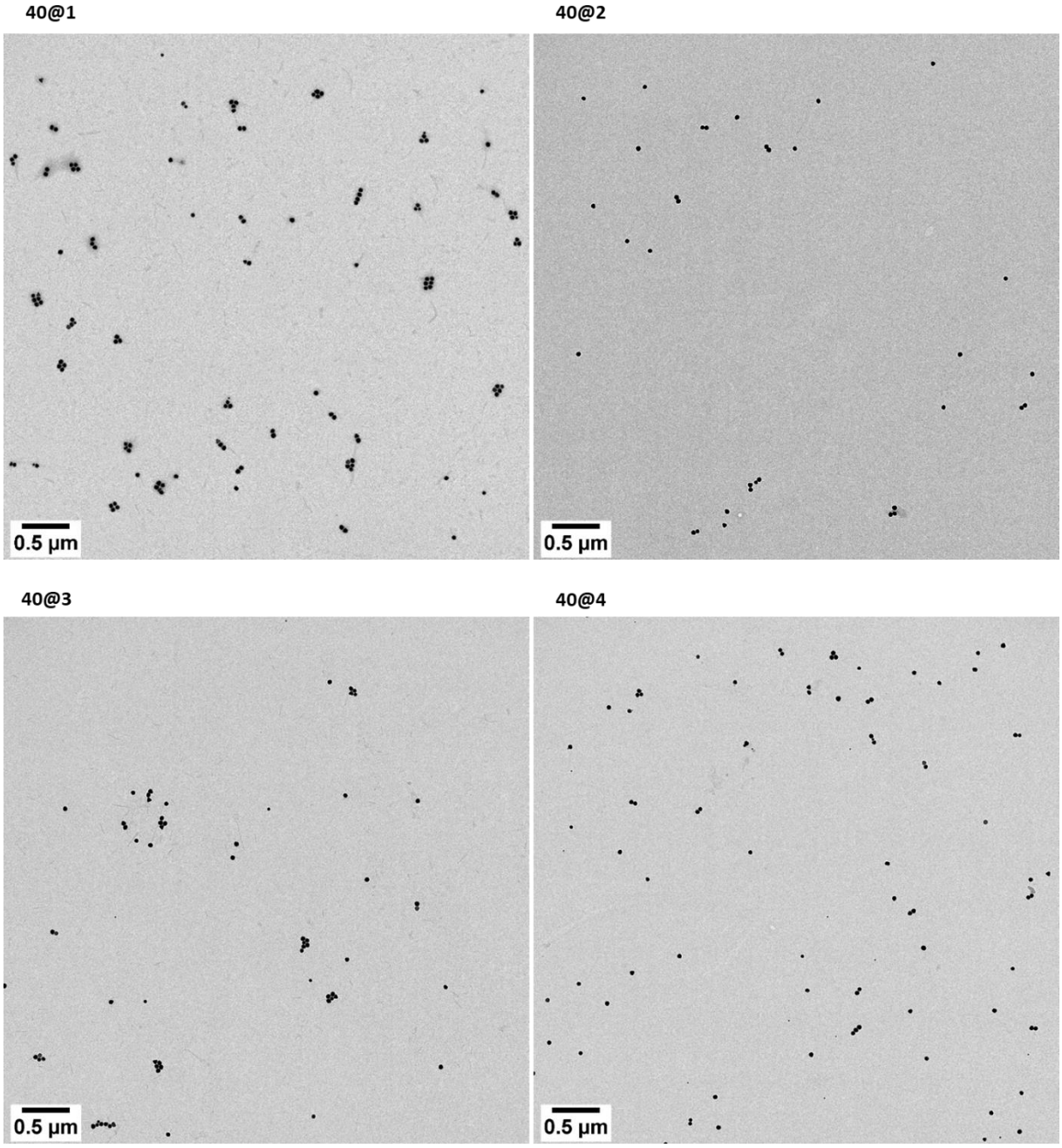

Figure S7. Representative low magnification images of 40 nm GNPs coated with molecules **1**-**4.**

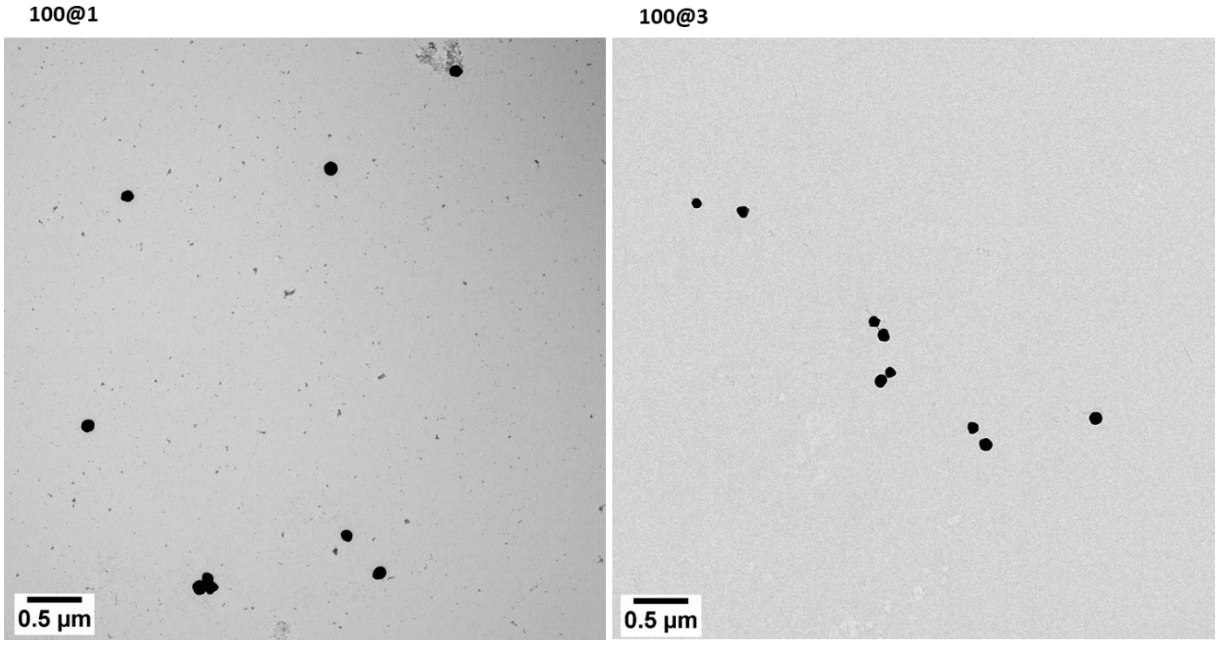

Figure S8. Representative low magnification images of 100 nm GNPs coated with molecules **1** and **3**.

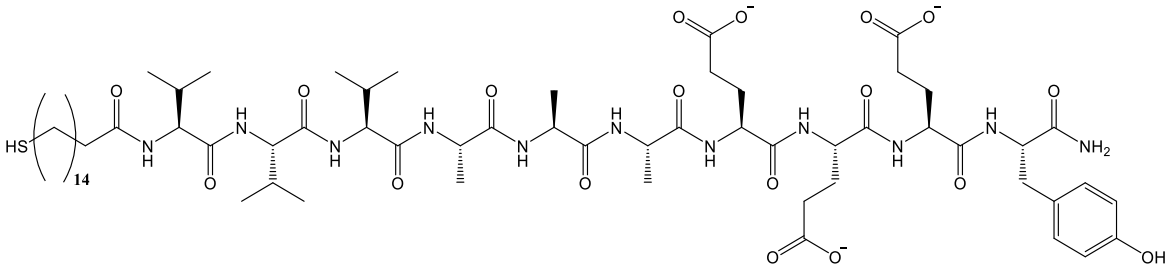

Scheme S1. Structure of the peptide used to evaluate coverage densities.

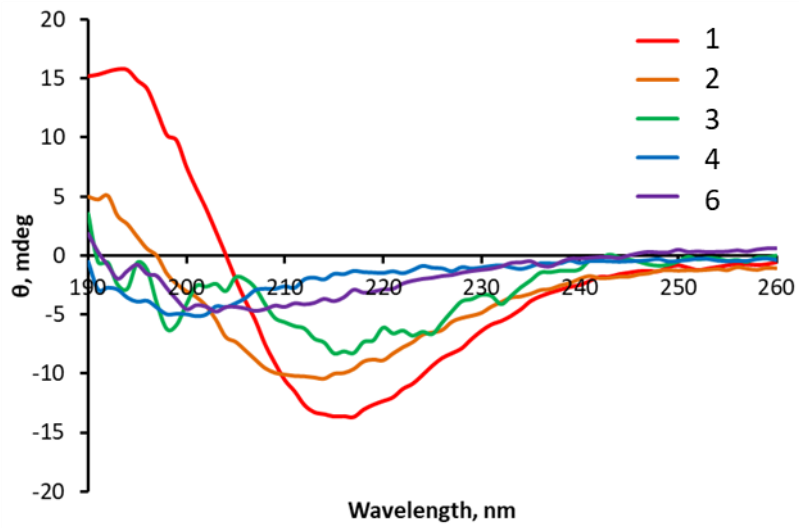

Figure S9. CD spectra of 20 nm coated GNPs illustrating the self-assembly of the amphiphilic molecules on the gold surface.
Conditions: [GNP] = 6 nM, PBS pH 7.2.

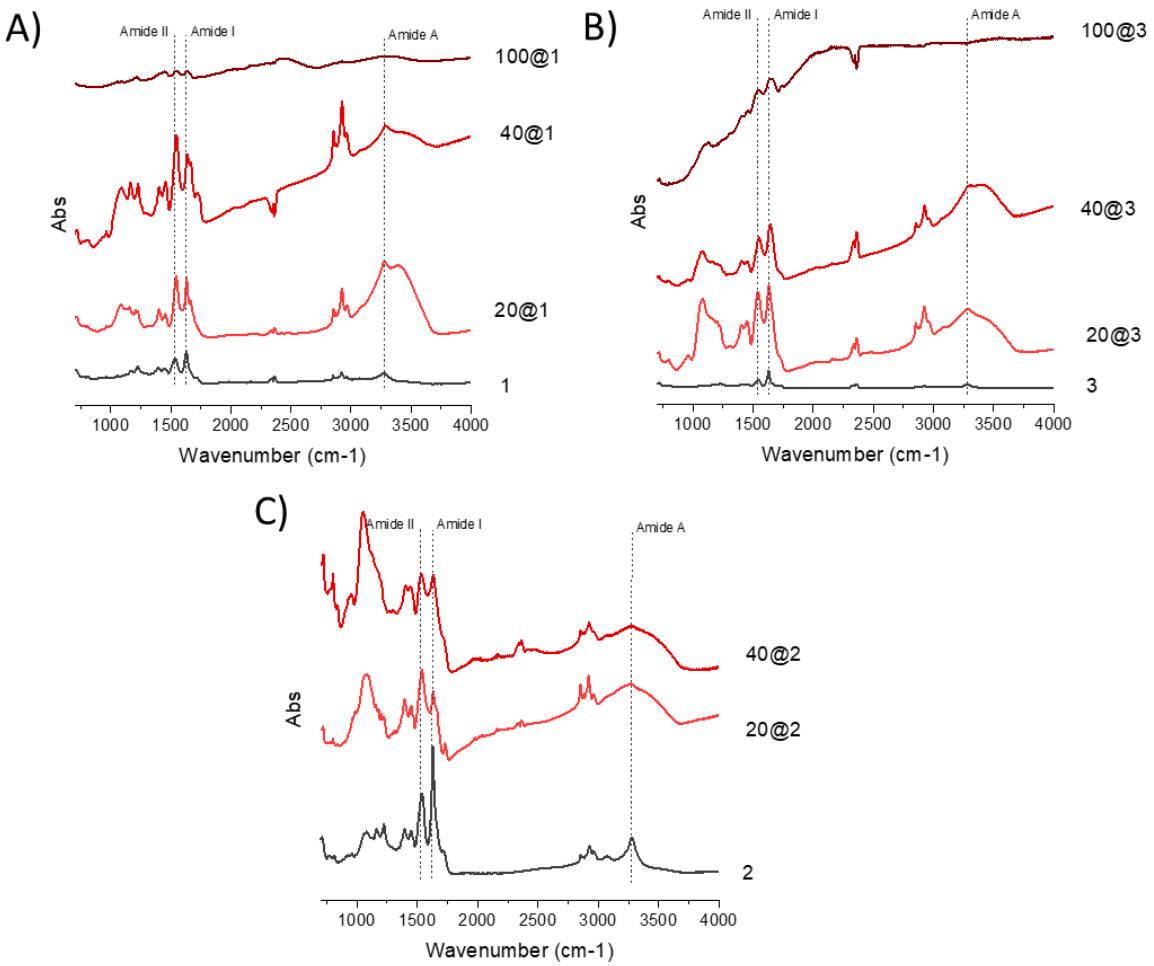

Figure S10. Full ATR-IR spectra of amphiphiles: (A) **1**, (B) **3**, and (C) **2**.

Table S3. Secondary structure percentages for amphiphiles in isolation and when bound to the surface of 20, 40, and 100 nm GNPs.

Sample	β, %	α, %	others, %
1	97.7	0	2.3
20@1	73.8	13.1	13.1
40@1	41.8	38.6	19.6
100@1	54.0	35.7	10.3
3	94.8	0.8	4.4
20@3	72.5	7.7	19.8
40@3	60.9	31.4	7.7
100@3	29.0	29.9	41.1
2	85.2	5.4	9.4
20@2	70.4	19.4	10.2
40@2	76.9	23.1	

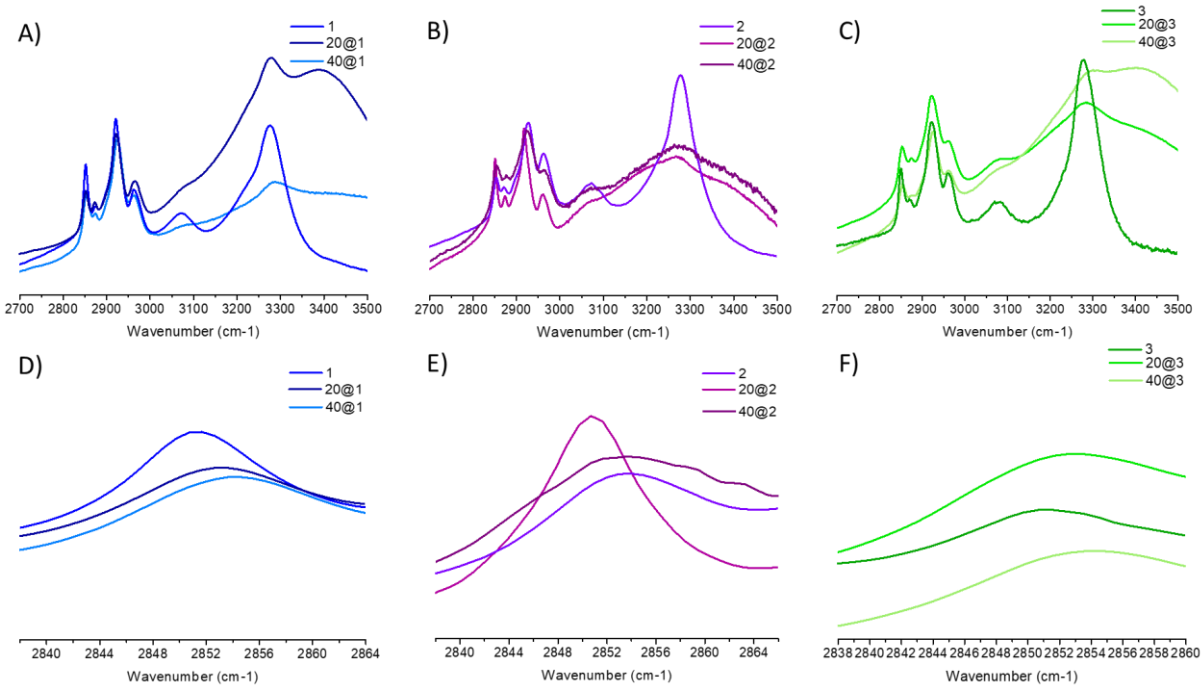

Figure S11. ATR-IR spectra in the range 2700-3500 cm^{-1} (A-C) and a close-up of the -CH_2- vibrational peak of the alkyl chain (D-F). Spectra are shown for the molecules by themselves and on 20 and 40 nm GNPs. For 100 nm GNPs it was not possible to distinguish individual peaks in this region due to a low intensity and high signal-to-noise ratio.

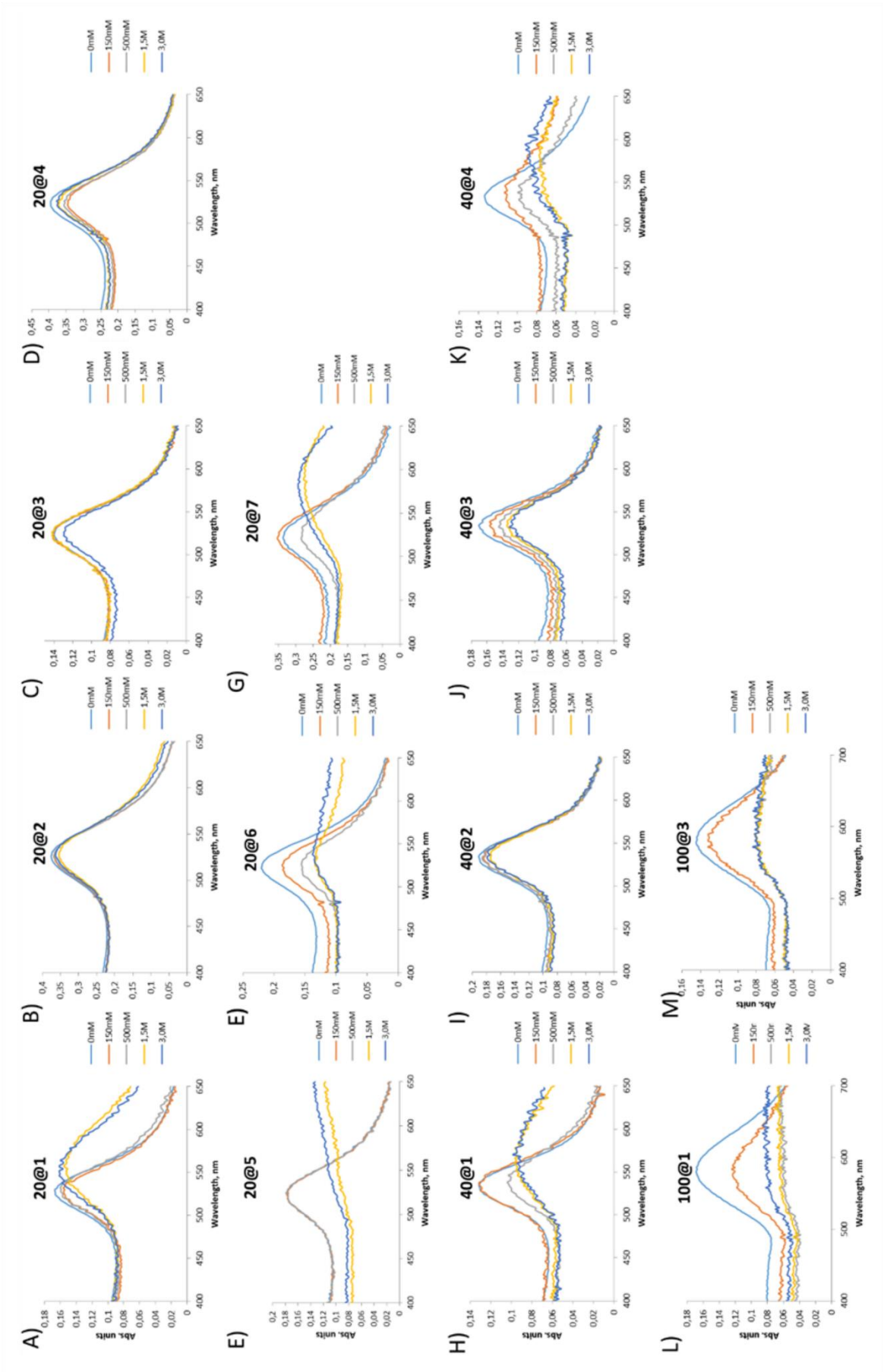

Figure S12. Overlays of UV-Vis spectra for 20, 40 and 100 nm GNPs coated with different stabilizing molecules at different concentrations of NaCl.

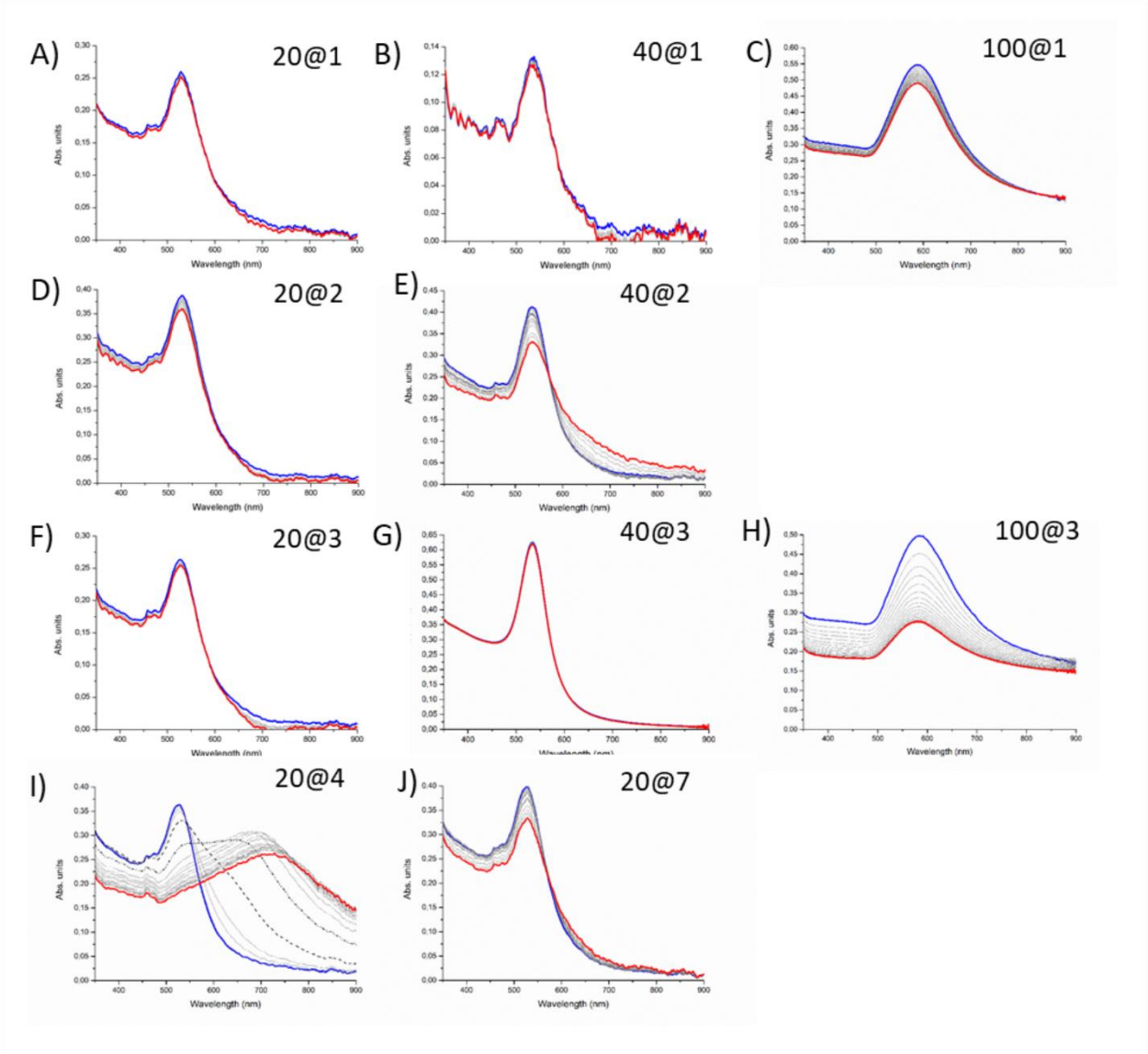

Figure S13. UV-Vis spectra for the DTT competition experiment with: (A) **1** on 20 nm GNPs; (B) **1** on 40 nm GNPs; (C) **1** on 100 nm GNPs; (D) **2** on 20 nm GNPs; (E) **2** on 40 nm GNPs; (F) **3** on 20 nm GNPs; (G) **3** on 40 nm GNPs; (H) **3** on 100 nm GNPs; (I) **4** on 20 nm GNPs, and; (J) **7** on 20 nm GNPs.

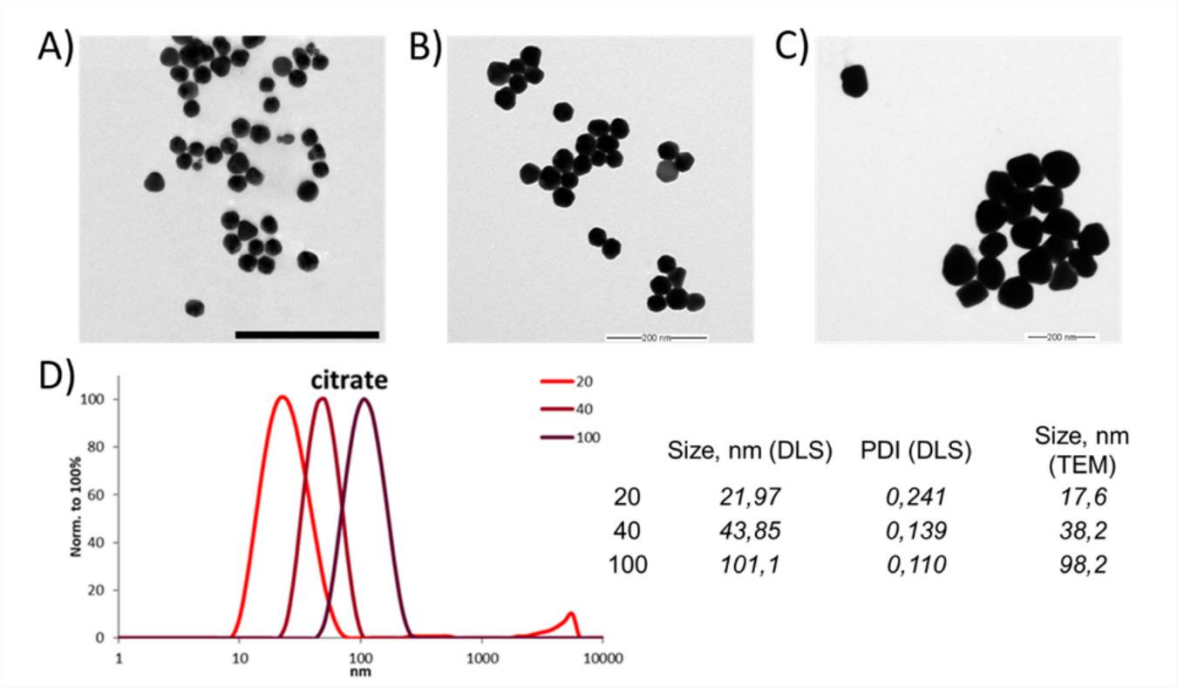

	Size, nm (DLS)	PDI (DLS)	Size, nm (TEM)
20	*21,97*	*0,241*	*17,6*
40	*43,85*	*0,139*	*38,2*
100	*101,1*	*0,110*	*98,2*

Figure S14. Size data for citrate-capped GNPs. TEM micrographs for (A) 20 nm GNPS, (B) 40 nm GNPs, and (C) 100 nm GNPs. (D) DLS data showing the size distributions for citrate-capped GNPs. The average sizes of the GNPs as determined by both DLS and TEM are shown in the table.

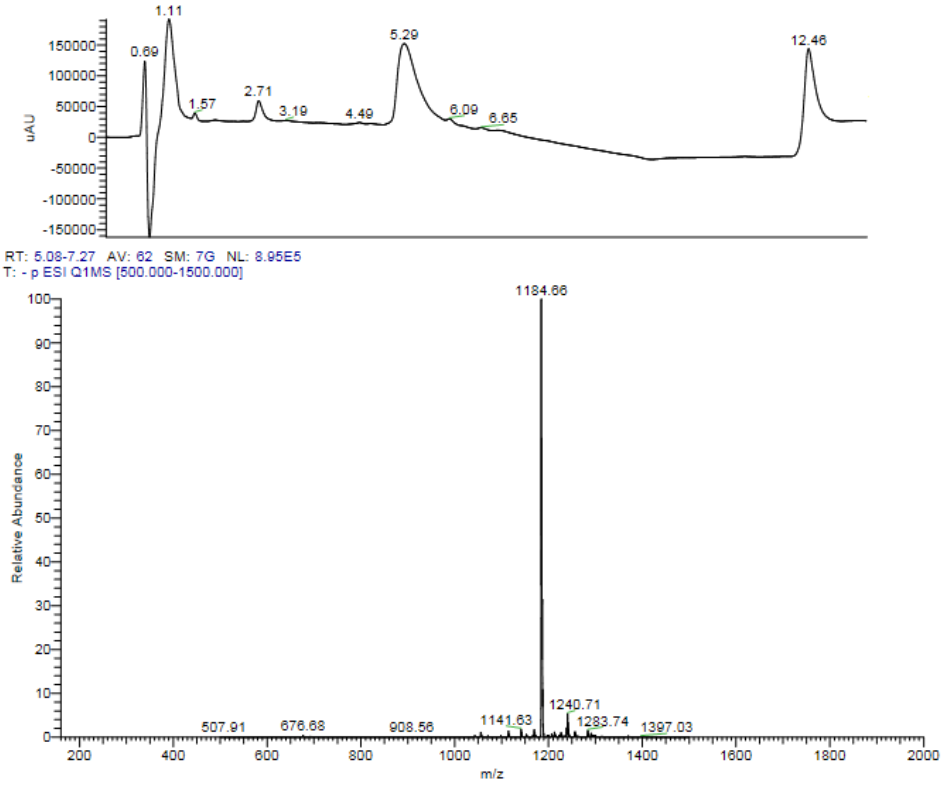

Figure S15. LC-MS spectrum for **1**: HS-$C_{16}H_{30}O$-$V_3A_3E_3$-OH

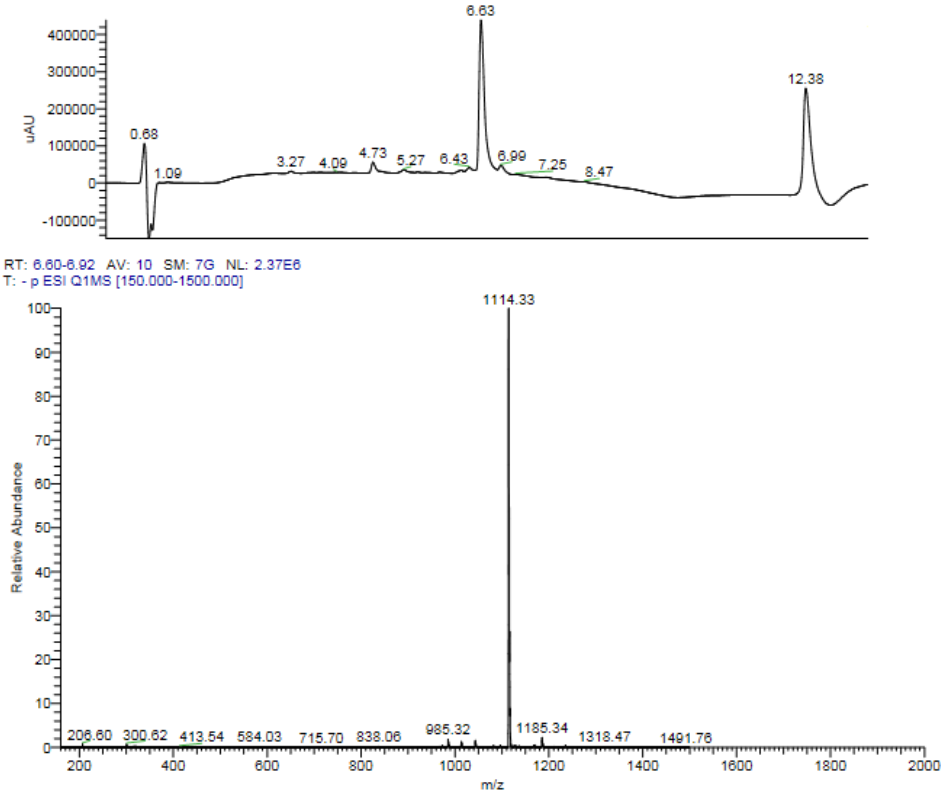

Figure S16. LC-MS spectrum for **2**: HS-$C_{11}H_{20}O$-$V_3A_3E_3$ -OH

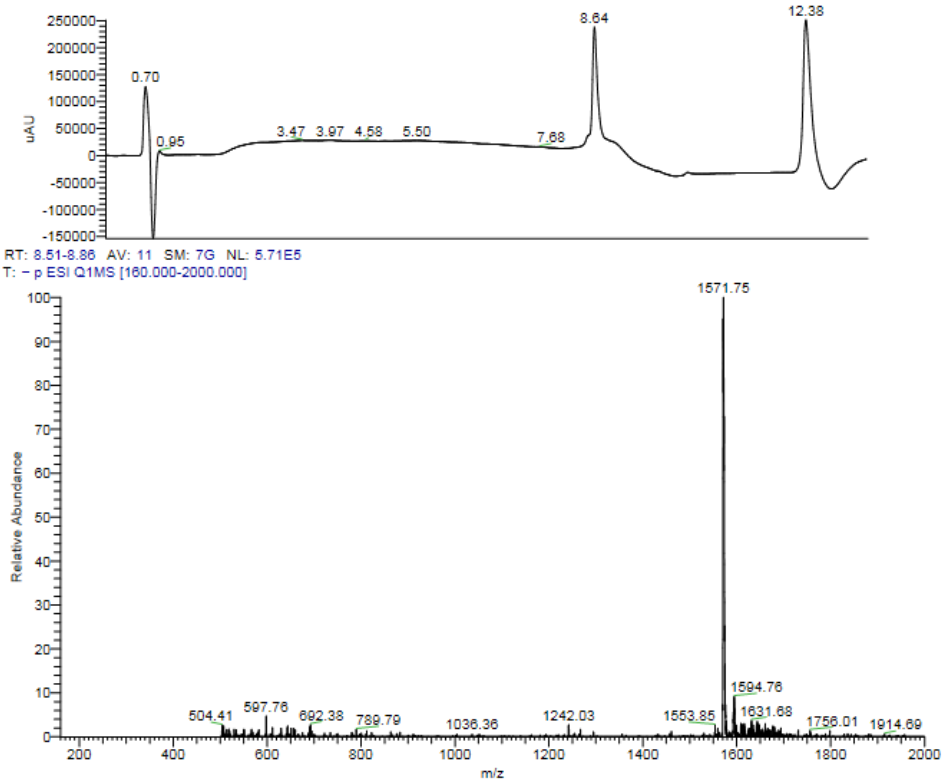

Figure S17. LC-MS spectrum for **3**: $(HS\text{-}C_{11}H_{20}O)_2\text{-}KV_3A_3E_4\text{-}OH$

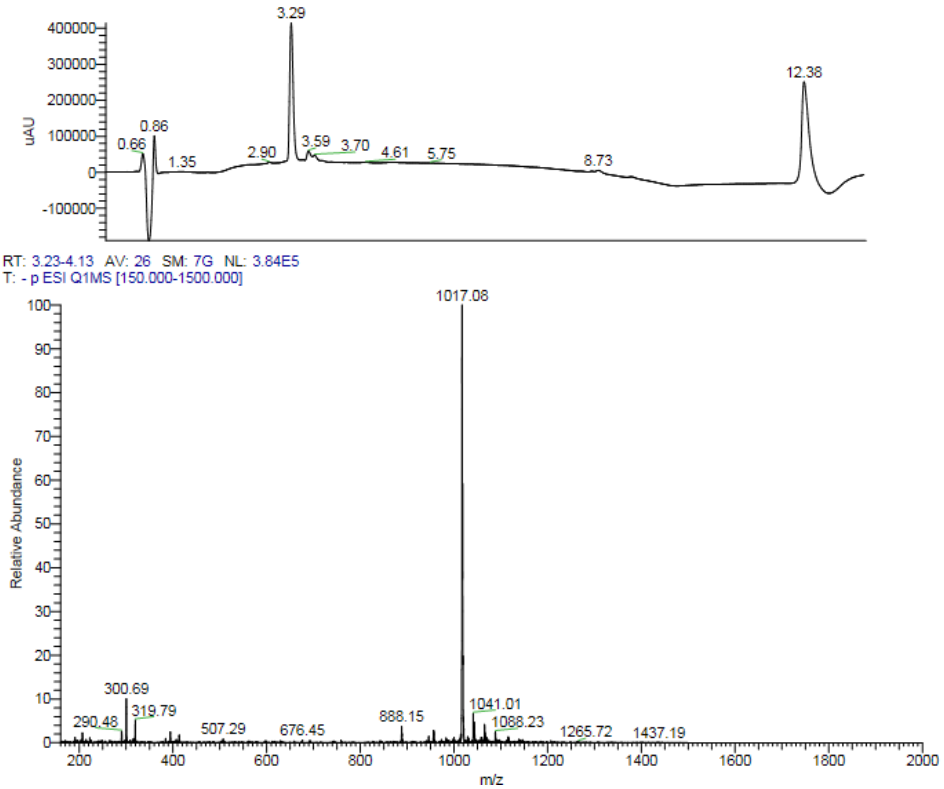

Figure S18. LC-MS spectrum for **4**: $H_2N\text{-}CV_3A_3E_3\text{-}OH$

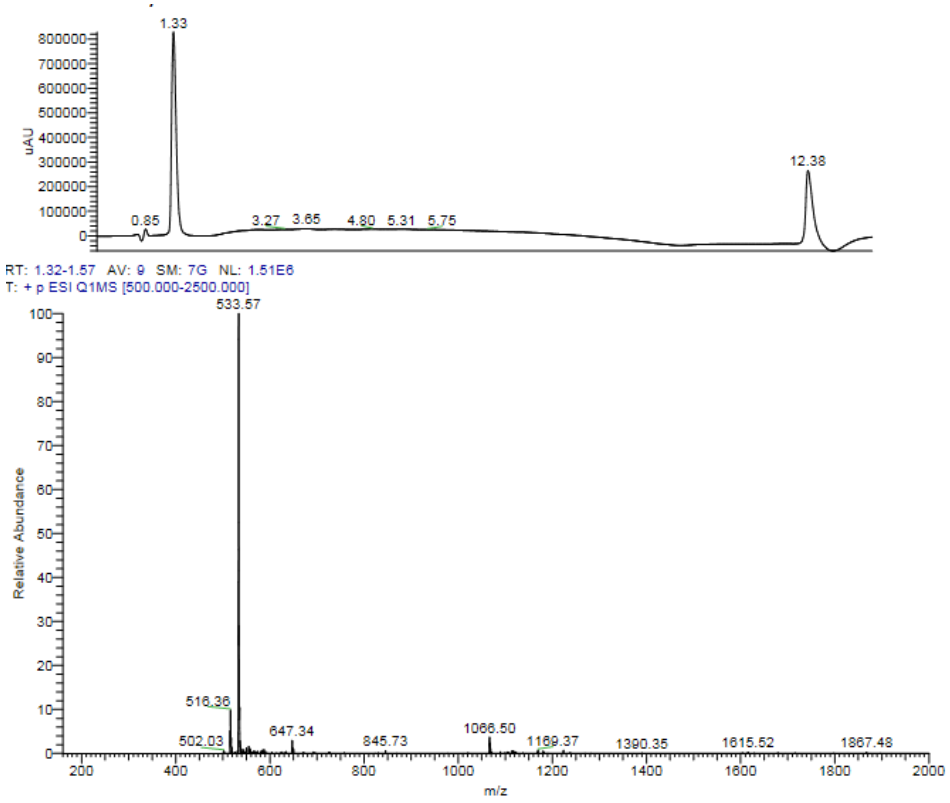

Figure S19. LC-MS spectrum for **5**: H_2N-CALNN-OH

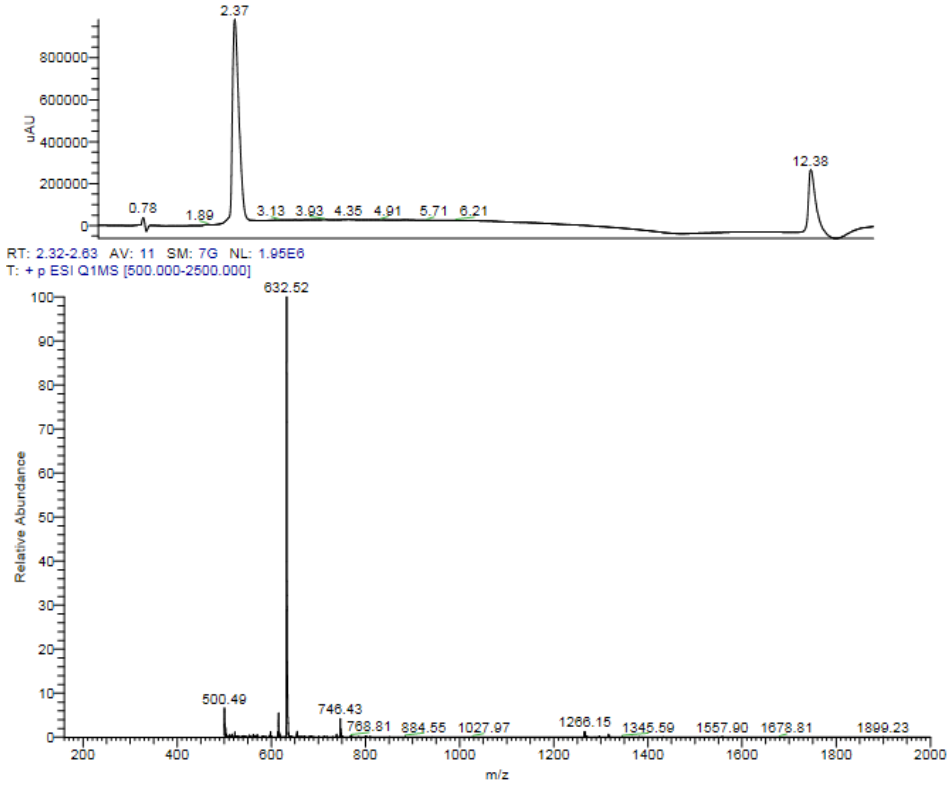

Figure S20. LC-MS spectrum for **6**: H_2N-CVALNN-OH

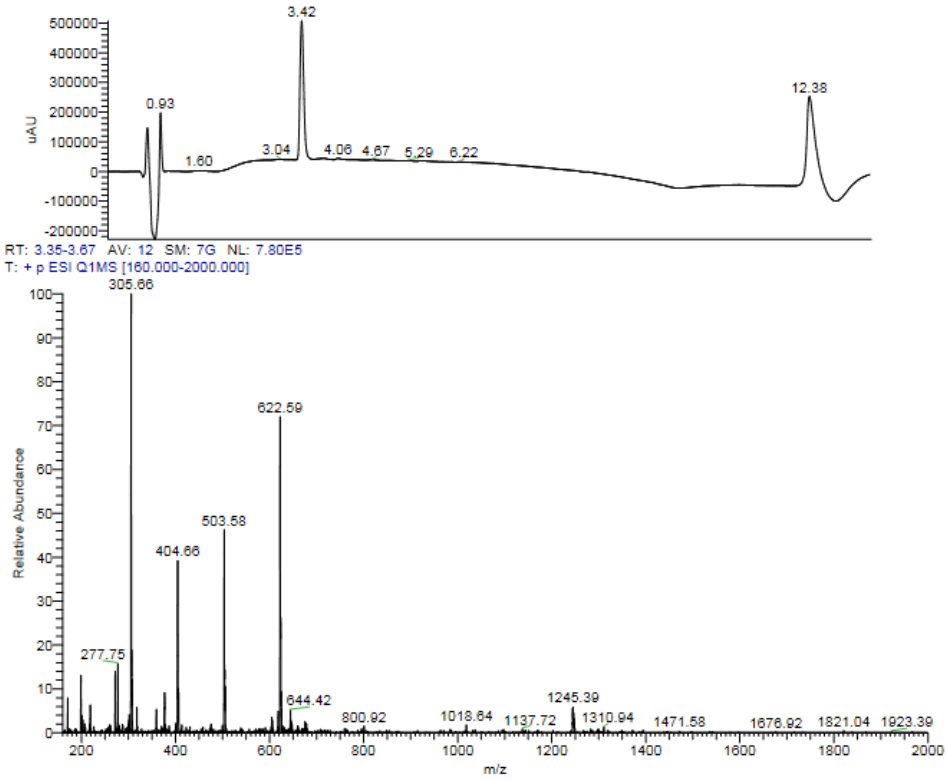

Figure S21. LC-MS spectrum for **7**: H_2N-CCVVVT-OH

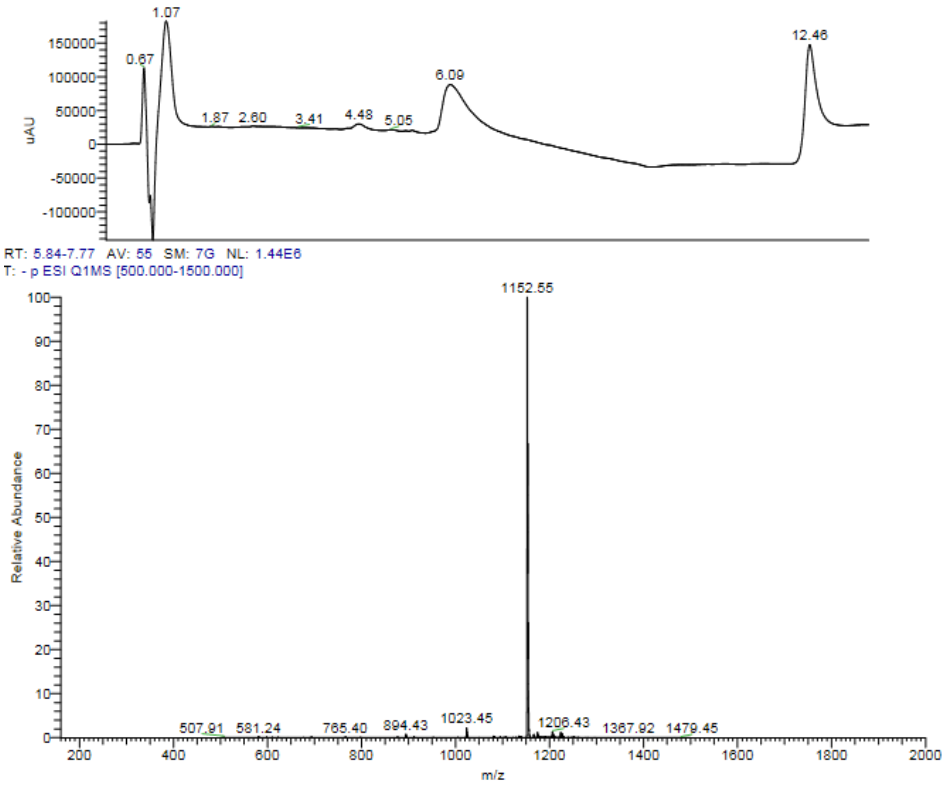

Figure S22. LC-MS spectrum for $C_{16}H_{31}O$-$V_3A_3E_3$-OH

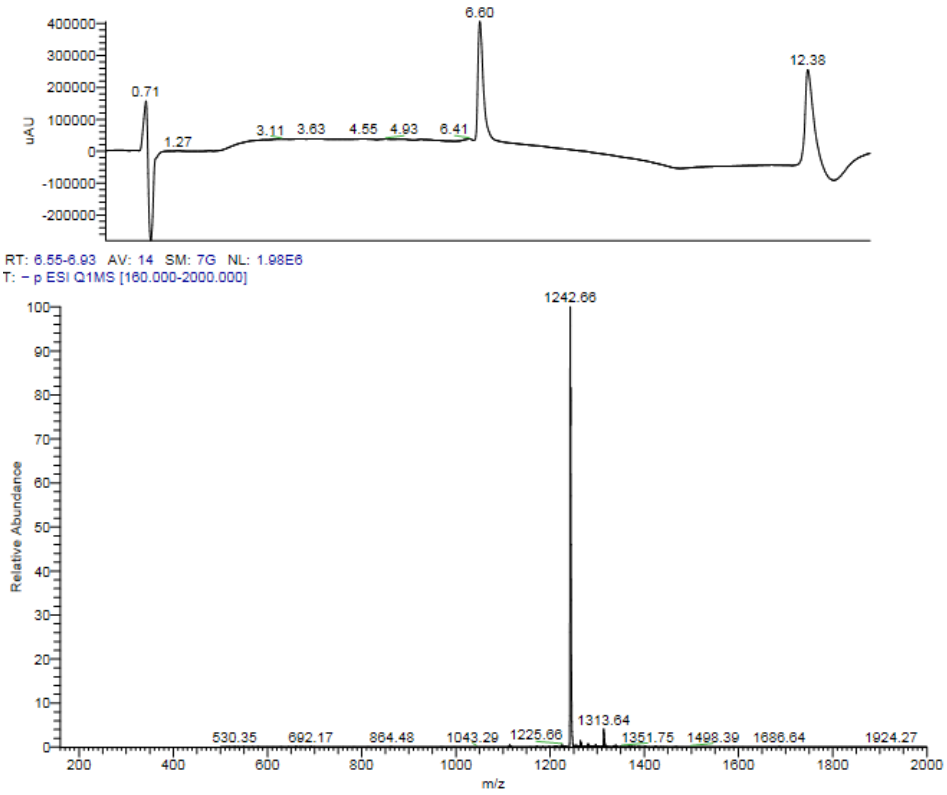

Figure S23. LC-MS spectrum for HS-$C_{11}H_{20}O$-$V_3A_3E_4$-OH

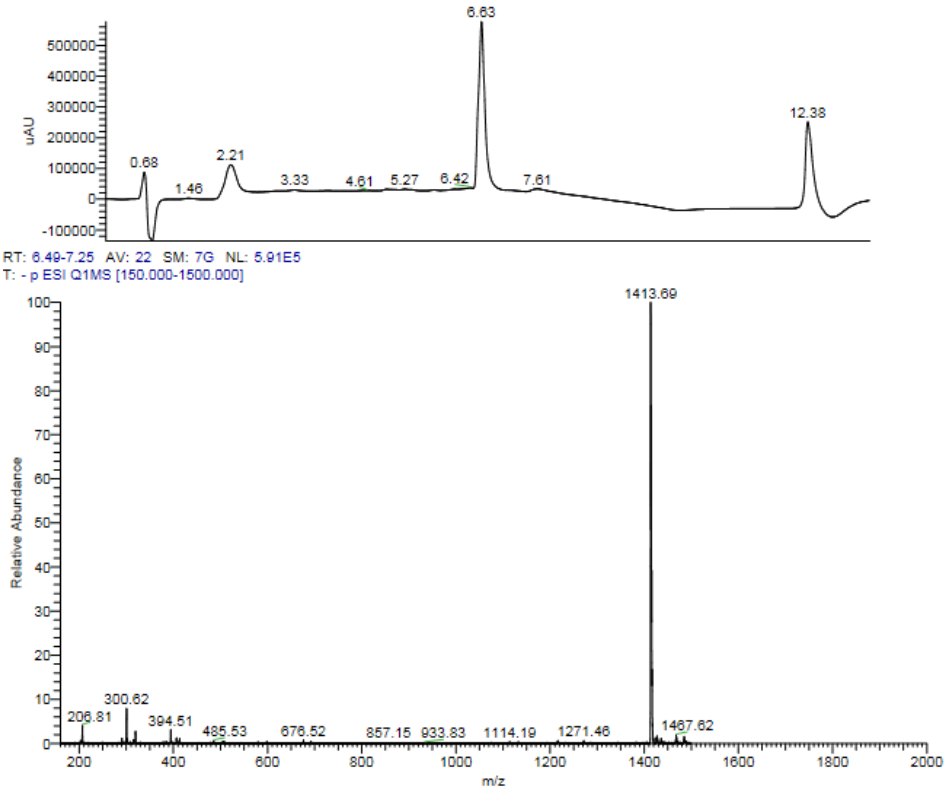

Figure S24. LC-MS spectrum for: HS-$C_{11}H_{20}O$-$K^{Ac}V_3A_3E_4$-OH

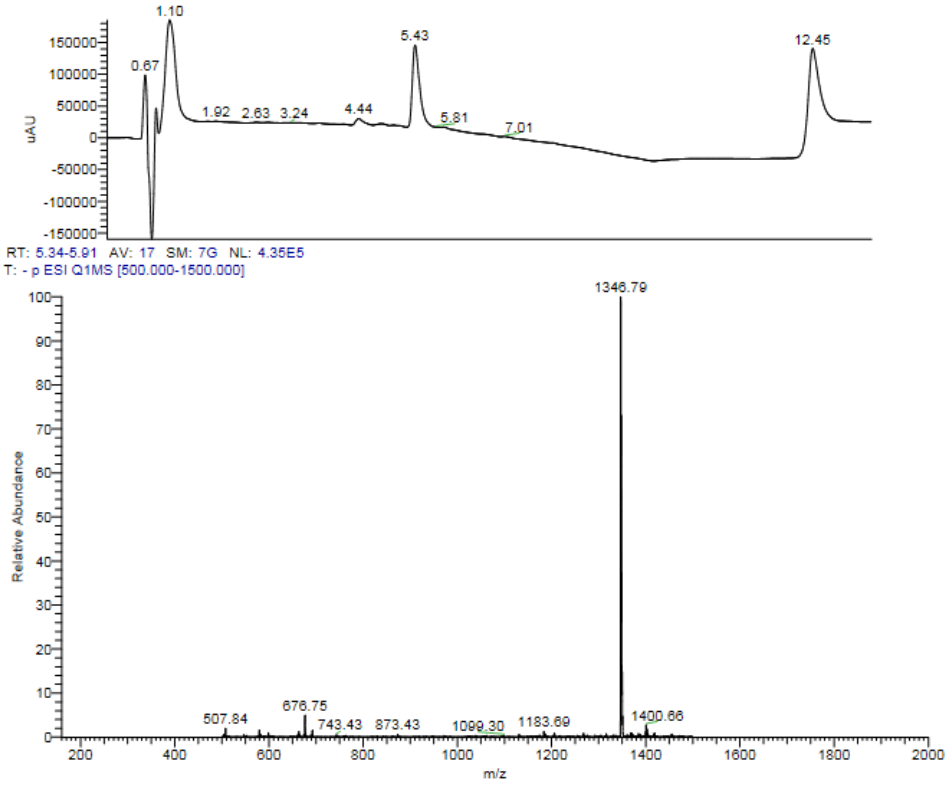

Figure S25. LC-MS spectrum for: HS-$C_{16}H_{30}O$-$V_3A_3E_3Y$-OH

References

1. Levy, R.; Thanh, N. T.; Doty, R. C.; Hussain, I.; Nichols, R. J.; Schiffrin, D. J.; Brust, M.; Fernig, D. G., Rational and Combinatorial Design of Peptide Capping Ligands for Gold Nanoparticles. *J. Am. Chem. Soc.* **2004**, *126*, 10076-10084.

2. Pashuck, E. T.; Cui, H.; Stupp, S. I., Tuning Supramolecular Rigidity of Peptide Fibers through Molecular Structure. *J. Am. Chem. Soc.* **2010**, *132*, 6041-6046.